Cerebral Glucose Metabolism

4

Wolf-Dieter Heiss and Olivier Zaro-Weber

Contents

Abstract

Glucose is the main substrate for energy metabolism of the brain, and the regional cerebral metabolic rate is directly related to regional brain activity. Therefore, the measurement of regional glucose metabolism is of great importance for the assessment of regional normal function and of pathological changes. Quantitation of glucose metabolism by PET is based on the 2-deoxyglucose method developed by Sokoloff and colleagues: F18-labelled deoxyglucose (FDG) is transported into the brain and phosphorylated, but cannot be further metabolised and therefore is accumulated intracellularly. The concentration of the tracer can be

W.-D. Heiss (✉)
Max Planck Institute for Neurological Research, Cologne, Germany
e-mail: wdh@nf.mpg.de

O. Zaro-Weber
Max Planck Institute for Neurological Research, Cologne, Germany

Department of Neurology and Center for Stroke Research Berlin (CSB), Charité – Universitätsmedizin, Berlin, Germany
e-mail: zaroweber@nf.mpg.de

R. A. J. O. Dierckx et al. (eds.), *PET and SPECT of Neurobiological Systems*,
https://doi.org/10.1007/978-3-030-53176-8_4

measured three dimensionally by PET, and together with the arterial tracer concentration, the kinetics of glucose uptake can be assessed, and the regional cerebral metabolic rates for glucose (rCMRGlc) can be calculated.

rCMRGlc is high in cortex and grey matter structures and low in white matter, but there are significant differences among various regions. Metabolic rate is slightly reduced with ageing and changed by sleep, dream, and functional activation. CMRGlc is significantly affected in pathological states, and the regional and global changes are important for assessing the severity of disorders and for differential diagnosis of diseases of the brain. Therefore, FDG-PET has still great importance in brain research and many applications in clinical neurology.

4.1 Energy Requirements of Brain Tissue

The energy demand of the nervous tissue is very high, and therefore sufficient blood supply to the brain must be maintained consistently. A normal adult male's brain containing approximately 130 billion neurons (21.5 billion in the neocortex) (Pakkenberg and Gundersen 1997) comprises only 2% of the total body mass yet consumes at rest approximately 20% of the body's total basal oxygen consumption supplied by 16% of the cardiac blood output. The brain's oxygen consumption is almost entirely for the oxidative metabolism of glucose, which in normal physiological conditions is the almost exclusive substrate for the brain's energy metabolism (Clarke and Sokoloff 1999). It must be kept in mind that the glucose metabolised in neuronal cell bodies is mainly to support cellular vegetative and housekeeping functions, e.g. axonal transport, biosynthesis of nucleic acids, proteins, lipids, as well as other energy-consuming processes not related directly to action potentials. Therefore, the rate of glucose consumption of neuronal cell bodies is essentially unaffected by neuronal functional activation. Increases in glucose consumption (and regional blood flow) evoked by functional activation are confined to synapse-rich regions, i.e. neuropil which contains axonal terminals, dendritic processes, and also astrocytic processes that envelope the synapses. The magnitudes of these increases are linearly related to the frequency of action potentials in the afferent pathways, and increases in the projection zones occur regardless of whether the pathway is excitatory or inhibitory. Only at the next downstream projection zones glucose utilisation (and, as a consequence, blood supply) is depressed in inhibited neurons and increased in excited neurons. Energy metabolism by functional activation is due mostly to the stimulation of the Na + K + −ATPase activity to restore the ionic gradients across the cell membrane and the membrane potentials that were degraded by the spike activity and is rather high compared to the demand of neuronal cell bodies (Sokoloff 1999). Overall, 87% of the total energy consumed is required by signalling, mainly action potential propagation and postsynaptic ion fluxes, and only 13% is expended in maintaining membrane resting potential (Attwell and Laughlin 2001).

4.2 Brain Energy Metabolism

Glucose is the obligatory energy substrate for the brain, and it is almost entirely oxidised to CO_2 and H_2O. Although the brain represents only 2% of the body weight, it receives 15% of the cardiac output, 20% of the total body oxygen consumption, and 25% of the total body glucose utilisation (Villien et al. 2014). With a global blood flow of 57 mL/100 g min, the brain extracts approximately 50% of oxygen and 10% of glucose from the arterial blood. Hence, the glucose utilisation of the brain, as assessed by measuring the arterial-venous difference (Kety and Schmidt 1948), is 31 mmol/100 g min. Oxygen consumption is 160 mmol/100 g min; because CO_2 production is almost identical, the respiratory quotient (RQ) of the brain is nearly 1, indicating that carbohydrates are the substrates for oxidative metabolism (Sokoloff 1989). Given a theoretical stoichiometry of 6 mmol of oxygen consumed for each mmole of glucose, glucose utilisation by the brain should in theory be 26.6 mmol/100 g min. As indicated earlier, the measured glucose utilisation is 31 mmol/100 g min, indicating that an excess of 4.4 mmol/100 g min of glucose follows other metabolic fates. Glucose can produce metabolic intermediates, such as lactate and pyruvate, which do not enter necessarily in the tricarboxylic acid cycle, but rather can be released and removed by circulation. Glucose can be incorporated into lipids, proteins, and glycogen, and it is also the precursor of certain neurotransmitters such as gamma-aminobutyric acid (GABA), glutamate, and acetylcholine (Sokoloff 1989).

Of molecules that could substitute for glucose as an alternative substrate for brain energy metabolism, mannose is the only one that can sustain normal brain function in the absence of glucose. Lactate and pyruvate can sustain synaptic activity in vitro. Because of their limited permeability across the blood–brain barrier, they cannot substitute for plasma glucose to maintain brain function (Pardridge and Oldendorf 1977). However, if formed inside the brain parenchyma, they are useful metabolic substrates for neural cells (review in Magistretti and Allaman 2015).

Whole-organ studies, which allowed the determination of the substrate requirements for the brain, failed to provide the appropriate level of resolution to appreciate two major features of brain energy metabolism: (a) its regional heterogeneity and (b) its tight relationship with the functional activation of specific pathways. The autoradiographic 2-deoxyglucose (2-DG) method developed by Sokoloff and colleagues afforded a sensitive means to measure local cerebral metabolic rates of glucose (LCMRGlc) with a spatial resolution of approximately 50–100 μm (Sokoloff et al. 1977). The method is based on the fact that tracer amounts of radioactive 2-DG are taken up by glucose transporters and phosphorylated by hexokinase with kinetics that are similar to those for glucose; however, unlike glucose-6-phosphate, 2-deoxyglucose-6-phosphate cannot be metabolised further and therefore accumulates intracellularly, thus providing, after appropriate corrections (Sokoloff et al. 1977), an accurate measurement of the amount of glucose utilised. Using this method, LCMRGlc have been determined in virtually all morphologically and

functionally defined brain structures in various physiological and pathological states including sleep, seizures, and dehydration and following a variety of pharmacological treatments. Furthermore, the increase in glucose utilisation following activation of pathways subserving specific modalities, such as visual, auditory, olfactory, or somatosensory stimulations, as well as during motor activity, has been revealed in the pertinent brain structures.

Basal glucose utilisation of the grey matter as determined by the 2-DG technique varies, depending on the brain structure, between 50 and 150 μmol/100 g wet weight/min in the rat (Sokoloff et al. 1977). Physiological activation of specific pathways results in a 1.5–3-fold increase in LCMRGlc as determined by the 2-DG technique.

With the advent of PET and the use of positron-emitting isotopes such as ^{18}F, local glucose utilisation has been studied in humans with 2-(^{18}F)fluoro-2-deoxyglucose (Reivich et al. 1979). Changes in local brain energy metabolism can now be studied in humans with PET by monitoring alterations in glucose utilisation, oxygen consumption, and blood flow during activation of specific areas. Studies in which these three parameters have been analysed during activation of a given modality have yielded an uncoupling between glucose uptake and oxygen consumption during activation, since the increase in blood flow and in glucose utilisation in the activated cortical area was not matched by an equivalent increase in oxygen consumption (Fox et al. 1988; Madsen et al. 1995; Blomqvist et al. 1994). This observation raises the puzzling possibility that, at least during the early stages of activation, the increased energy demand is met by glycolysis rather than by oxidative phosphorylation (Vaishnavi et al. 2010; Raichle and Mintun 2006).

4.2.1 Glycolysis and Oxidative Phosphorylation

Glycolysis (Embden–Meyerhof pathway) is the metabolism of glucose to pyruvate and lactate. It results in the net production of only 2 mol of adenosine triphosphate (ATP)/mol of glucose as well as in the regeneration of reducing equivalents (the oxidised form of nicotinamide adenine dinucleotide (NAD+)) through the conversion of pyruvate into lactate. Alternatively, pyruvate can enter the tricarboxylic acid (TCA) cycle (or the Krebs cycle) and produce 30 mol of ATP/mol of glucose via the mitochondrial oxidative phosphorylation cascade. The energetic value of oxidative phosphorylation over glycolysis is thus obvious. The respiratory quotient of the brain is virtually 1; PET studies indicate an uncoupling between glucose uptake and oxygen consumption during activation (Fox et al. 1988; Madsen et al. 1995), and rises in lactate have been monitored. During activation, lactate may normally be taken up by neurons as an energy fuel. It should be remembered that after conversion to pyruvate, lactate can enter the TCA cycle with the potential to generate a total of 36 mol of ATP/mol of glucose. Activation-induced glycolysis may provide ATP to fuel energy-dependent ion transport, in particular the Na+/K + −ATPase, which represents the main energy-consuming process in neural cells (Siesjo 1978).

4.2.2 Determination of the Regional Cerebral Metabolic Rate for Glucose (rCMRGlc)

The study of glucose metabolism with 18FDG is a direct application of the autoradiographic technique of Sokoloff et al. (1977) with [^{14}C]deoxyglucose. The model developed by Sokoloff et al. can be applied directly because the fluorodeoxyglucose labelled at point 2 behaves in the same way as deoxyglucose. It is transported into the cell in the same way as glucose and, with the aid of hexokinase, is phosphorylated to [^{18}F]deoxyglucose-6-phosphate. Deoxyglucose-6-phosphate, however, cannot be further converted to fructose-6-phosphate and degraded to CO_2 and H_2O, but accumulates in the cell. The kinetics of the back reaction (phosphatase) to deoxyglucose is much slower, and the deoxyglucose-6-phosphate can penetrate through the cell membrane only in small amounts. The kinetics of the accumulation of deoxyglucose-6-phosphate can be described with the transport and enzyme constants of a three-compartment model (Fig. 4.1). The corresponding complex formula (Reivich et al. 1979) for calculating the regional cerebral metabolic rate of glucose (rCMRGlc) (Fig. 4.2) can be simplified to the following form (Phelps et al. 1979):

$$\mathrm{rCMRGl} = \frac{(\mathrm{GI})}{\mathrm{LC}} \bullet \frac{\mathrm{C}\left(^{18}\mathrm{F}\right) - \mathrm{C}(\mathrm{FDG})}{A_b}$$

where C(^{18}F) is the total fluorine activity measured in the tissue, which is determined directly in the PET, and C(FDG) is the concentration of free FDG in the tissue, calculated from the plasma concentration up to time point T with the aid of the

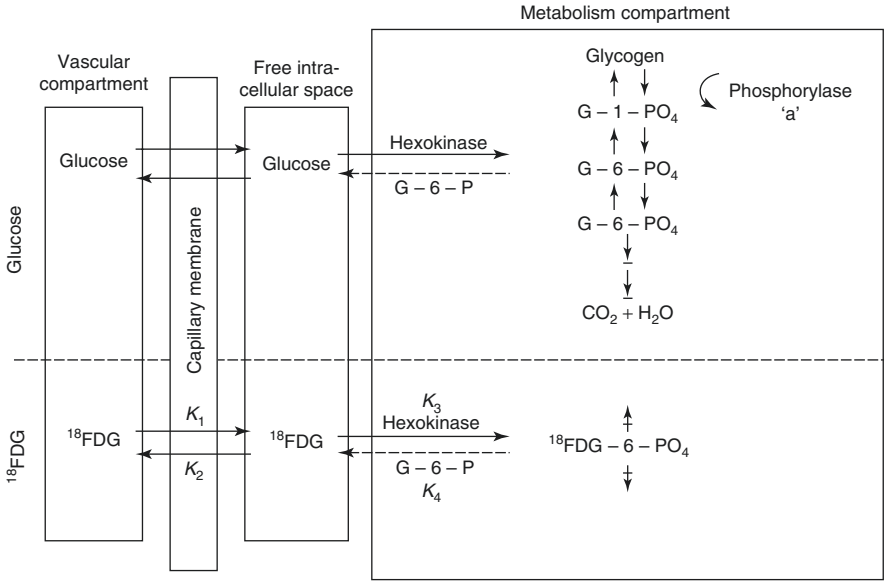

Fig. 4.1 Transport and metabolism of glucose and ^{18}F-FDG in brain tissue (see text for details)

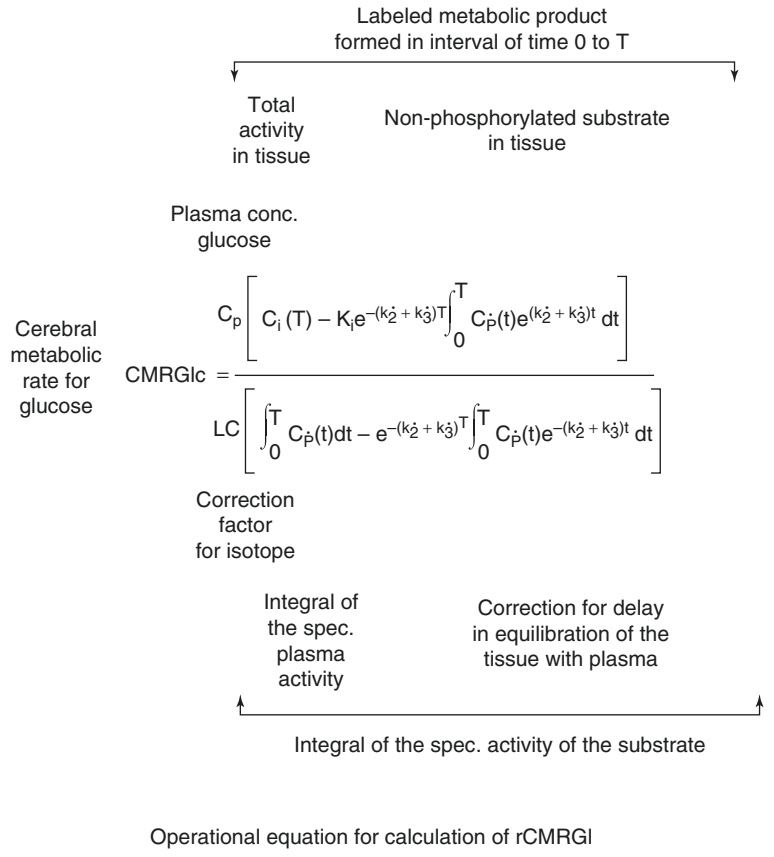

Fig. 4.2 Equation for calculation of regional cerebral metabolic rate of glucose (rCMRGlc) in the brain

constants of the model. The difference between these two values gives the local tissue concentration of FDG-6-phosphate; A_b is the total quantity of FDG released into the tissue and is calculated from the plasma FDG concentration curve up to time point *T*, decreased by the delay in the tissue equilibration using the corresponding model constants. The quotient therefore gives the proportional phosphorylation rate of FDG. Multiplication by the plasma concentration of glucose (Glc) would yield the rate of glucose phosphorylation if it behaved in the same way as FDG. Since the arterial-venous extraction of glucose is not identical with that of FDG, the value must be corrected with an experimentally determined constant (LC = lumped constant). For the measurement of the regional glucose consumption in the brain, therefore, after i.v. administration of 3–6 mCi 18FDG, the plasma curve of 18FDG from the injection to the measurement time point (usually determined in arterialised venous blood), the glucose value in plasma, and the regional ^{18}F activity in the brain must be determined.

Errors resulting with this model from widely diverging kinetic constants in pathological tissue (Hawkins et al. 1981) can be reduced by dynamic PET. For this purpose, the tissue activity is determined at short time intervals from the time point of injection. By variation of the values for the kinetic constants, the curve deriving from the model equation is adapted to the measured regional activity time curve. The kinetic constants thus determined correspond best to the activity uptake in the corresponding tissue segment. They allow the regional metabolic rate for glucose to be directly calculated (Wienhard et al. 1985). It is now only necessary to assume a known value for the LC.

There remains some uncertainty as to the exact value of the normal "lumped constant" (LC) for FDG. The initial value empirically derived by Phelps et al. (1979) was 0.42. It has been directly measured by Reivich et al. (1985), who found a value of 0.52, assuming $k_4 = 0$. But LC could be even as high as 0.65 (Wu et al. 2003). However, regional changes in LC are small. For the sake of uniformity, the actual value used should be quoted in all publications. This will allow direct comparison of numerical values because the LC is a linear scaling factor in the operational equations. With rate constants measured by dynamic curve fitting or by integration techniques, the equation for calculation of CMRGlc is:

$$\mathrm{CMRglc} = \mathrm{C_a} / \mathrm{LC} \times \left(k_1 k_3 / \left(k_2 + k_3 \right) \right)$$

The term $k_1k_3/(k_2 + k_3)$, representing the metabolic rate of FDG, can be substituted by the influx rate constant *ki* determined with the linear approximation of Patlak et al. (1983). There have also been modifications that avoid the assumption of a fixed LC and refer instead to the Michaelis–Menten equation to account for the relations between enzyme affinities for FDG and glucose (Kuwabara et al. 1990).

Determination of individual rate constants is not very practical in many clinical applications, and methods are preferred that can be done with a single scan, a situation similar to the original development of the method for autoradiography. Then the deviation from population average CMRGlc (given by the average rate constants) is estimated from a single scan. Actual measured FDG activity is compared with the activity that would have been expected at the time of the scan with the individual's blood activity time course and average rate constants (Wienhard et al. 1985).

To avoid the conversion factor needed with the analogue tracer FDG, native glucose labelled with 11C in the 1-position (1-11C-d-glucose) has also been used for quantitation of CMRGlc (Raichle et al. 1975). Modelling is based on the same two-tissue compartment model as with FDG, but an additional term is necessary to account for labelled metabolites (mainly lactate and other monocarboxylic acids and CO_2). Metabolites occur in the plasma and in the brain, and loss of labelled CO_2 from the brain is dependent on CBF. Data indicate that there is a rapid loss of labelled lactate from the brain, suggesting that it represents a significant nonoxidative part of glucose metabolism in the brain (approximately 10% of the total CMRGlc) (Blomqvist et al. 1990).

4.2.3 Normal Glucose Consumption of the Brain

In healthy volunteers, a mean glucose consumption of 29–32 μmol/100 g/min was found by means of FDG and PET (Reivich et al. 1979; Heiss et al. 1984), which correspond well to whole-brain metabolic rates provided by the Kety–Schmidt method. Under controlled conditions (darkened laboratory and steady noise from fans of equipment cooling systems), the functional anatomy of the brain is reflected in the metabolic activity of the individual regions. However, reliable regional values for cerebral metabolic rate of glucose (rCMRGlc) can only be obtained by equipment permitting high 3D resolution of tracer concentration in the brain tissue (Heiss et al. 2004). This progressively improved spatial resolution of PET is documented in Fig. 4.3 showing FDG images of the brain in the same volunteer assessed with different tomographs over the years (Heiss 2009a, b). Typical resting state grey matter CMRGlc values are in the range of 40–60 μmol/100 g/min, and the corresponding level in the white matter is about 15 μmol/100 g/min. There are significant differences among regions with highest values in the basal ganglia, primary visual cortex, and cingulate and frontal cortex (42–50 μmol/100 g/min) and lower values in other cortical and subcortical areas (35–42 μmol/100 g/min) and in the structures of the brain stem (25–30 μmol/100 g/min) and the cerebellum (33 μmol/100 g/min). There exist also significant asymmetries with largely right hemispheric predominance (Pawlik and Heiss 1989), review in Silverman and Melega (2004). The resting regional metabolism and its asymmetry are highly dependent on the state of resting wakefulness (e.g. apprehensive or relaxed) and background conditions (e.g. laboratory noise).

Local CMRGlc measured with PET is influenced by age: glucose metabolism of various grey matter structures was low at birth (13–25 μmol/100 g/min), reached a level of 19–33 μmol/100 g/min by 2 years and continued to rise until age 3–4 years, and was maintained at a high level (49–55 μmol/100 g/min) until age of 10 years (Chugani et al. 1987). At about 10 years, CMRGlc began to decline with a rather uniform decrease by 26% in all investigated brain regions of 40 healthy resting subjects between the ages of 18 and 78 years (Kuhl et al. 1982). However, these age-dependent changes were not observed in all studies (Duara et al. 1984). In our own study on 42 normal subjects aged 15–85 years, a small (0.65 μmol/100 g/min per decade/$p < 0.05$) age-dependent decrease in global CMRGlc was found (Fig. 4.4). However, as demonstrated in Fig. 4.4, the various regions contributed differently to this overall effect: decreases of 16.6–11.3% in cingulate, frontal, parietal, insular, temporal, and sensorimotor cortex, virtually no change in the primary visual cortex and cerebellum (Pawlik and Heiss 1989). Similar age-dependent changes of rCMRGlc were described in further studies (Kalpouzos et al. 2009; Hsieh et al. 2012; Chetelat et al. 2013; Berti et al. 2014; Shen et al. 2012; Bonte et al. 2017; Jiang et al. 2018).

Hardly any normal functional state is as regularly associated with as dramatic changes of general behaviour and shifting of attention as is sleep. The conclusion of no effect of sleep on human cerebral haemodynamics and metabolism, derived from early Kety–Schmidt studies (Mangold et al. 1955), could be disproved with PET (Heiss et al. 1985). As shown in Fig. 4.5, during stages II–IV sleep, a significant ($P < 0.001$) global decrease of brain functional activity was observed, with the

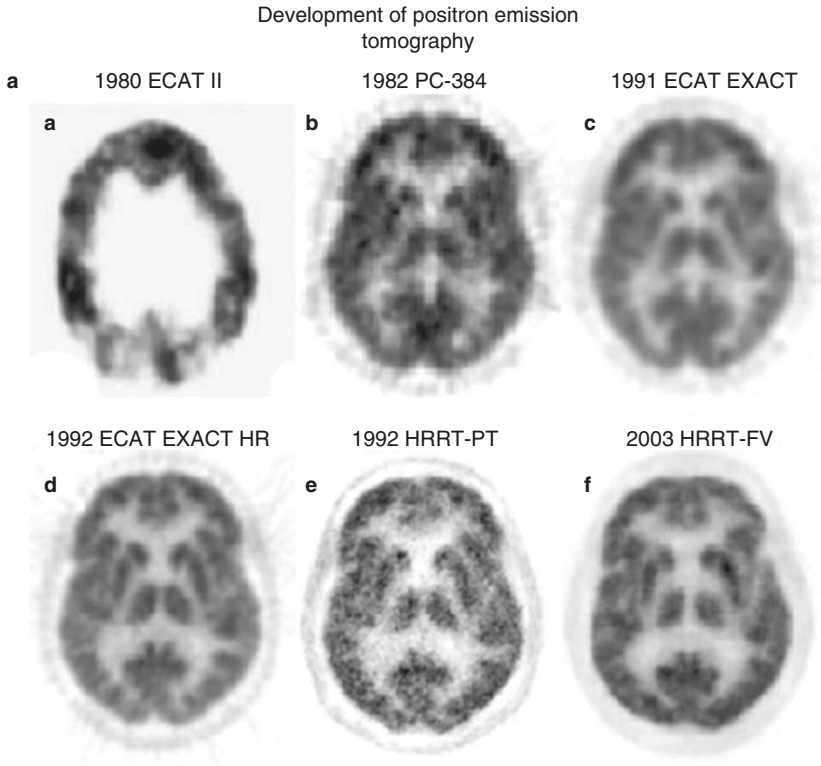

Fig. 4.3 (**a**) Development of PET: a horizontal slice. Various PET systems over the years demonstrate improvement in image quality and spatial resolution. (*a*) ECAT II, spatial resolution 15 mm. (*b*) PC-384, FWHM 8.4 mm. (*c*) ECAT EXACT, FWHM 6.5–7 mm. (*d*) ECAT EXACT HR, FWHM 3.6–4.5 mm. (*e*) *f* HRRT PET: *e* prototype. (*f*) final version (HRRT-FV), FWHM 2.3–3.2 mm. Images of glucose metabolism were acquired for 20 min of steady-state starting 30 min after tracer administration. (**b**) Coronal views of glucose consumption of the brain in a volunteer acquired with various PET systems over the years demonstrate improvement in axial resolution due to decreased slice thickness and advances in image reconstruction. (*a*) ECAT II (1980) was a single-ring camera; axial reconstruction was therefore not feasible. (*b*) PC-384, slice thickness 12 mm. (*c*) ECAT EXACT, axial FWHM 5–8 mm. (*d*) ECAT EXACT HR, axial FWHM 4.0–6.7 mm. (*e*) *f* HRRT PET: *e* prototype. (*f*) final version (HRRT-FV), axial FWHM 2.5–3.4 mm

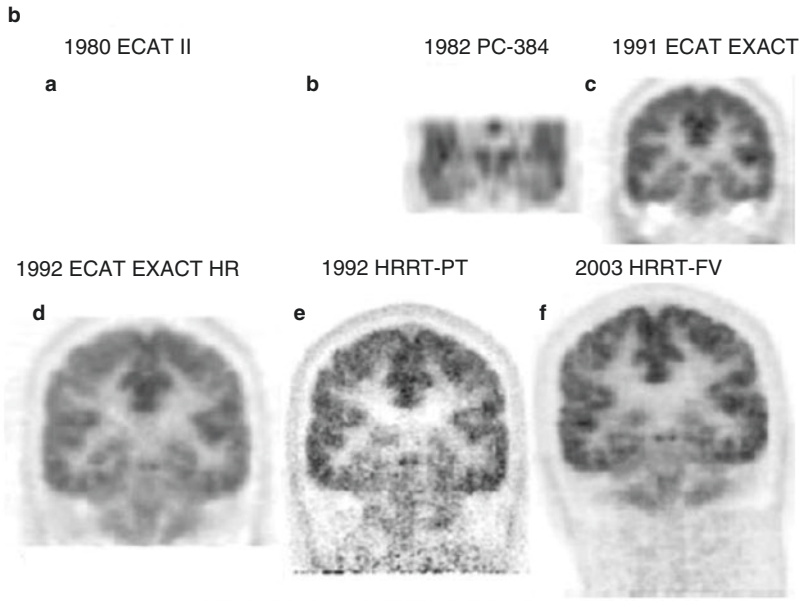

Fig. 4.3 (continued)

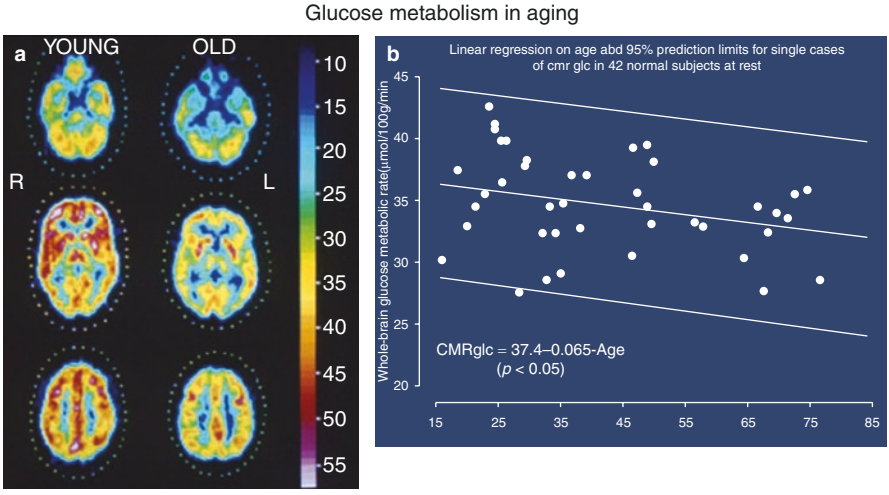

Fig. 4.4 (**a**) PET scans of glucose metabolism (µmol/100 g/min according to scale) in cerebral sections at the level of the cerebellum, basal ganglia, thalamus, and semioval centre in young (23 years) and old (67 years) healthy subjects. The individual brain structures can be differentiated according to different metabolic rates; metabolism decreases slightly in all regions in older patients. (**b**) Decrease of mean global glucose metabolic rate in 42 healthy subjects with increasing age. The regression line shows a significant relationship despite the large range of variation

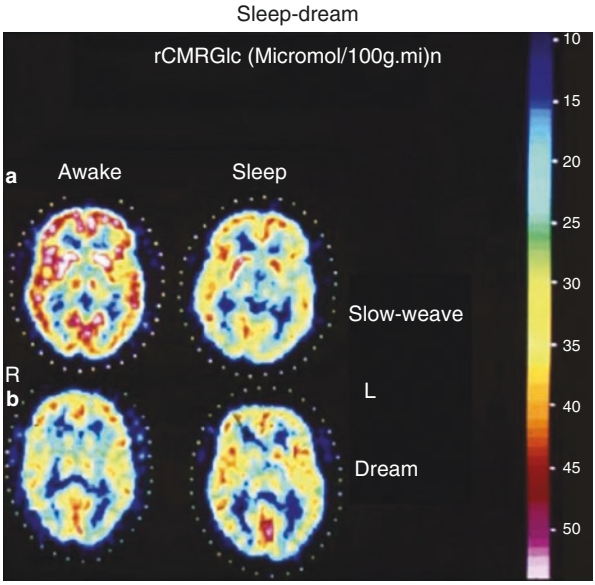

Fig. 4.5 (**a**) Corresponding images of the local cerebral metabolic rate for glucose determined by FDG-PET in a characteristic horizontal brain slice across the basal ganglia of a healthy 37-year-old male subject representative of the non-dreamers group, showing nonselective decrease in glucose utilisation from wakefulness (W) to sleep (S). Frontal poles are on top, occipital poles at bottom, sides as marked (R, L). Values on reference scale are in μmol/100 g min. (**b**) Corresponding metabolic maps of a 28-year-old normal volunteer's brain slice recorded by FDG-PET while the subject was awake (W) and asleep dreaming (S). A generalised activation, most marked in the insular regions, visual cortex, and hippocampal formations, is clearly demonstrated during sleep with dreaming

largest declines in the orbitofrontal cortex and in the thalamus. In dream sleep, by contrast, both a general metabolic increase and conspicuous regional activations of superior frontal, insular, inferior parietal, hippocampal, and visual association cortex (Heiss et al. 1985) were found. Increased CMRGlc during REM sleep has also been observed in limbic and paralimbic regions including hypothalamus, amygdala, orbitofrontal cingulate, entorhinal, and insular cortices (Nofzinger et al. 1997).

4.2.4 Coupling of Neuronal Activity to Metabolism and Flow

The activation of Na+, K +-ATPase represents the coupling mechanism between the increase in glucose utilisation and functional activity of the nervous tissue. The activation- induced increase in glucose uptake is visualised in the neuropil, that is, where synapses ensheathed by astrocytes are present, not at the level of the neuronal perikarya. Glucose, taken up by astrocytic processes, is metabolised glycolytically to lactate and pyruvate, which are then released as substrates for oxidative

phosphorylation in neurons (Wyss et al. 2011; Juaristi et al. 2019). Mapping of neuronal activity in the brain can be primarily achieved by quantitation of the regional cerebral metabolic rate for glucose (rCMRGlc), as introduced for autoradiographic experimental studies by Sokoloff (1977) and adapted for positron emission tomography (PET) in humans (Reivich et al. 1979). Functional mapping, as it is widely used now, relies primarily on the hemodynamic response assuming a close association between energy metabolism and blood flow. While it is well documented that increases in blood flow and glucose consumption are closely coupled during neuronal activation, the increase in oxygen consumption is considerably delayed leading to a decreased oxygen extraction fraction (OEF) during activation (Villien et al. 2014; Mintun et al. 2001). PET detects and, if required, can quantify changes in CBF and CMRGlc accompanying different activation states of the brain tissue. The regional values of CBF or CMRGlc represent the brain activity due to a specific state, task, or stimulus, in comparison to the resting condition, and colour-coded maps can be analysed or coregistered to morphologic images.

Due to the radioactivity of the necessary tracers, activation studies with PET are limited to a maximum of 12 doses of 15O-labelled tracers, e.g. 12 flow scans, or 2 doses of ^{18}F-labelled tracers, e.g. 2 metabolic scans. Especially for studies of glucose consumption, the time to metabolic equilibrium (20–40 min) as well as the time interval between measurements required for isotope decay (HT for ^{18}F 108 min, for 15O 2 min) must be taken into consideration. FDG-PET was the leading method to investigate functional activation in humans in the 1980s (Pawlik and Heiss 1989; Phelps et al. 1981). PET-FDG activation studies assess task-induced CMRGlc changes either by performing the bolus method, with one or two separate PET scans, or as described recently by constant infusion of FDG during the entire scan for rest and activation condition (Villien et al. 2014; Hahn et al. 2016). FDG activation studies can also be applied in patients with functional disorders due to localised brain damage, e.g. by stroke and tumour (review in Chiaravalloti et al. (2019)), and has found broad application to patients with aphasia (Heiss 2009a, b). An example is given in Fig. 4.6 showing different activation patterns in poststroke aphasia which are related to prognosis and recovery of language function.

4.2.5 Clinical Applications of FDG-PET

Since its introduction, FDG-PET has been applied for studying the pathophysiology and for differential diagnosis of several neurological and psychiatric disorders (Chiaravalloti et al. 2019; Herholz et al. 2013; Jones et al. 2012). These applications will be described in the special clinical chapters of this book series. Some examples where FDG-PET has gained special importance are shown here.

In dementias, FDG-PET has attained a special role to detect progression of regional functional disturbance related to severity of cognitive and memory impairment (Fig. 4.7) and for differential diagnosis to other degenerative disorders

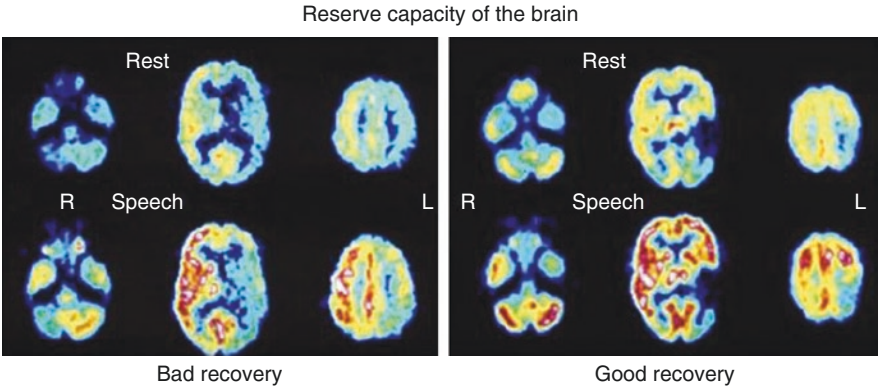

Fig. 4.6 Resting and speech-activated regional glucose metabolism in two patients with aphasia after ischemic stroke: if only contralateral regions are activated by speech, the prognosis is poor. If activation takes also place in homolateral periinfarct regions, prognosis is better, and speech performance shows satisfactory recovery

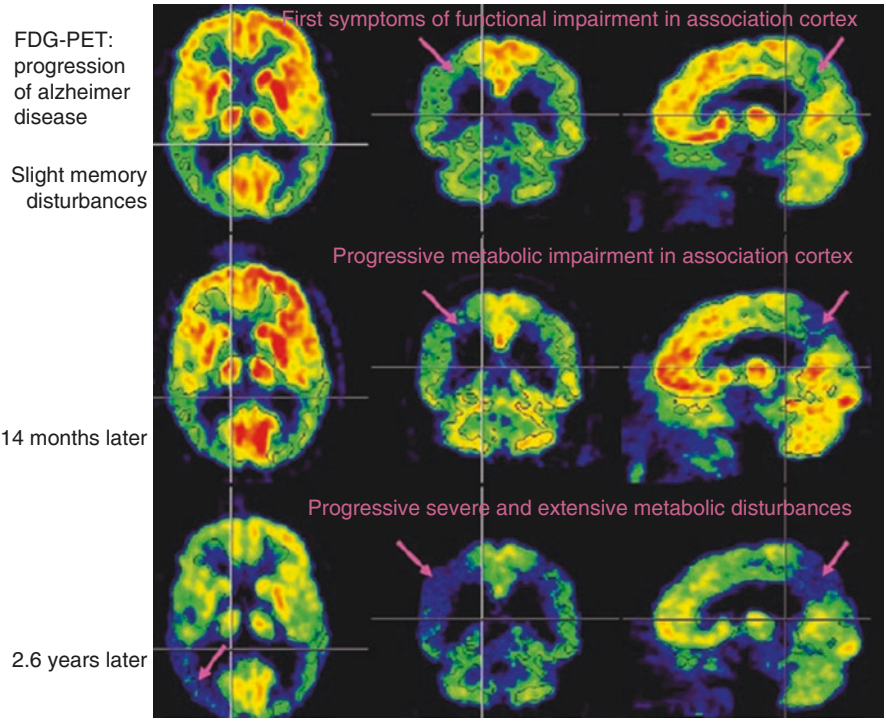

Fig. 4.7 Decline of cerebral metabolic rate (glucose) (CMRGlc) in association areas with progression of AD from the clinical stage of mild cognitive impairment (MCI) to mild dementia (three follow-up FDG-PET scans, each showing the same orthogonal slices at position marked by crosshairs)

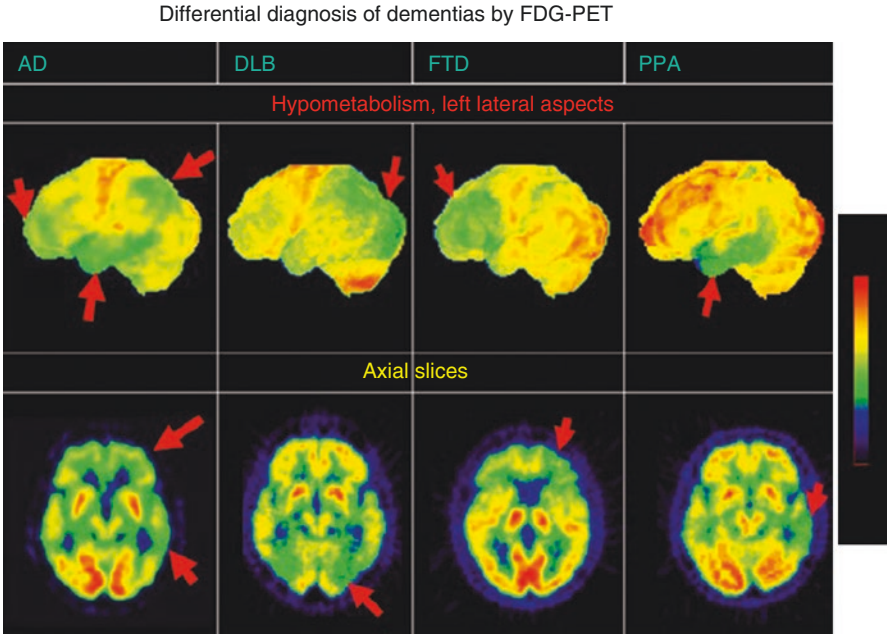

Fig. 4.8 FDG-PET in the differential diagnosis of various degenerative dementias. *Upper row*: typical transaxial slices. *Lower row*: reconstructed surface view. *AD* Alzheimer dementia, characterised by the decreases in temporoparietal and temporal association and in cingulate cortex; *FTD* frontotemporal dementia, the metabolic decrease is most severe in the anterior frontal and temporal regions; *DLB* dementia with Lewy body (Parkinson's disease), the metabolic disturbance also affects the visual cortex; *PPA* primary progressive aphasia, the disturbance is most accentuated in the temporal (Wernicke) area. *Arrows* indicate most prominent changes

(Fig. 4.8) and to vascular dementia (Fig. 4.9) (Drzezga 2009; Drzezga et al. 2018; Heiss and Zimmermann-Meinzingen 2012; Heiss 2018; Bohnen et al. 2012; Choo et al. 2013; Garibotto et al. 2017).

In brain tumours, FDG-PET has been successful in differentiating between necrosis and recurrent tumour (Fig. 4.10) and has value for grading of gliomas and for assessing the effect of chemotherapy (Heiss et al. 2011; Chierichetti and Pizzolato 2012; Herholz 2017; Herholz et al. 2012).

FDG-PET is the most common tracer used in epilepsy since epileptogenic foci are hypometabolic on interictal imaging, and FDG imaging is a commonly used tool in presurgical assessment of epilepsies (von Oertzen 2018; Broski et al. 2018; Lotan et al. 2020).

FDG-PET imaging has also been extensively performed in Parkinson's disease and is able to distinguish between several other movement disorders (Meyer et al. 2017; Meles et al. 2020).

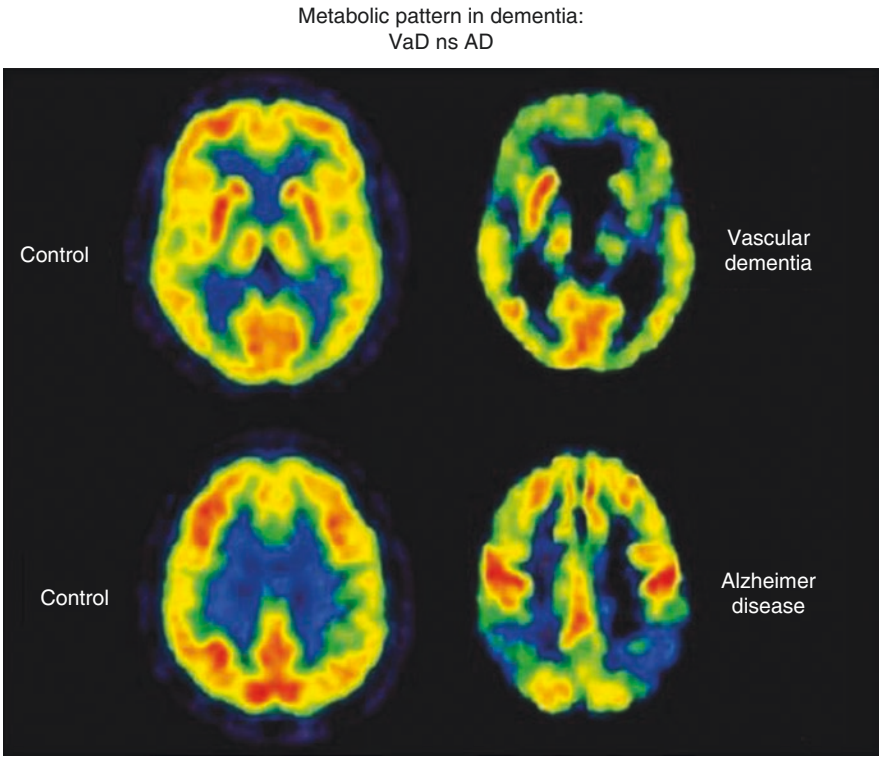

Fig. 4.9 Glucose metabolism in a normal control, in a patient with vascular dementia and a patient with Alzheimer's disease. The severity of dementia was comparable; the pattern of pathological changes differentiated these two cases: patchy metabolic defects in VaD in the frontal lobe, basal ganglia, and thalamus and hypometabolism in AD bilateral in parieto-temporal cortex and to a lesser degree in the frontal association areas, whereas primary cortical regions are spared

Neuroimaging of sleep disorders such as narcolepsy and primary hypersomnias with FDG-PET combined with other MR-based measures has given insight into the neural basis and pathogenesis of narcolepsy and primary or idiopathic hypersomnias (for review, see Cavaliere et al. 2020).

In ischemic stroke, 18FDG-PET has a role in discriminating recoverable ischemic brain tissue (penumbra) from infarcted tissue (infarct core) to predict along with 15O-PET tissue fate in acute and subacute ischemic stroke (Fig. 4.11) (Heiss et al. 1992; Nasu et al. 2002; Bunevicius et al. 2013).

Since plaque inflammation contributes to stroke and FDG identifies carotid plaque inflammation-related metabolism, FDG-PET is suitable to independently predict future recurrent stroke which may improve patient selection for revascularisation therapies as well as anti-inflammatory therapy (Marnane et al. 2012; Kelly et al. 2019).

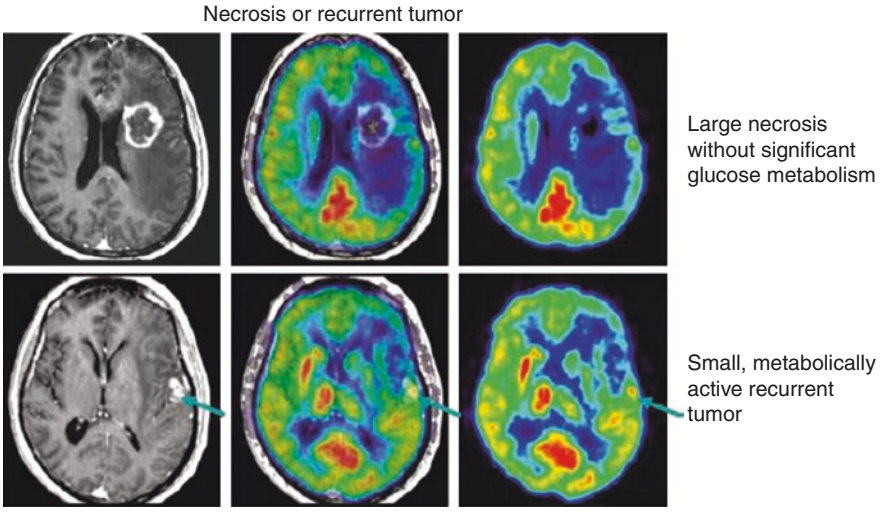

Fig. 4.10 FDG-PET and coregistered MRI in a patient with a large contrast-enhancing radiation necrosis (*top row*) and a small recurrent active carcinoma metastasis (*bottom row*)

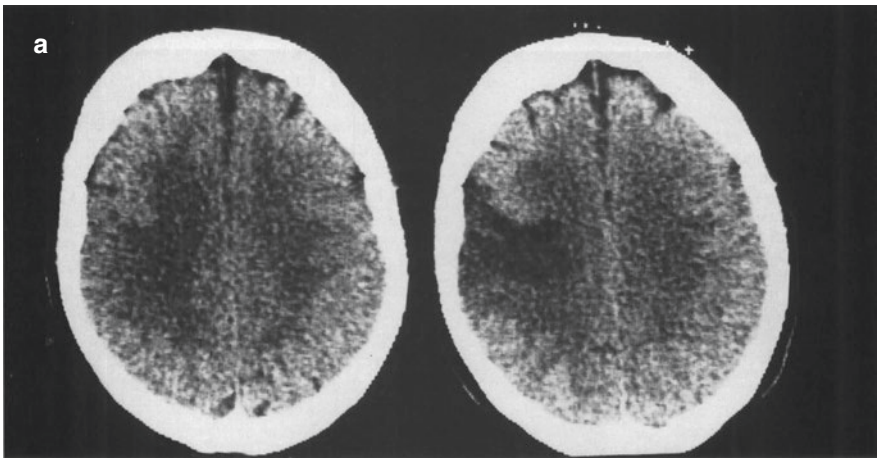

Fig. 4.11 CT and multitracer PET study of a patient 24 h after ischemic stroke in the territory of the right middle cerebral artery. CT and PET images of a brain slice 55 mm above the canthomeatal plane are presented. (**a**) While the initial CT is inconclusive, the ischemic infarct is clearly demarcated on the CT 4 days later. (**b**) PET images of the measured variables clearly demonstrate the flow defect (on CBF image) and the metabolic disturbance (CMRO2 and CMRGlc): the flow defect, however, is larger than the CMRO2 and CMRGlc defect, leaving border zone regions with preserved oxygen and glucose consumption and therefore increased oxygen extraction fraction (OEF) and glucose extraction fraction (GEF). This anterior portion is preserved at the later CT. In the posterior rim, however, CMRO2 is more severely impaired than CMRGlc leading to an increase in the ratio of glucose to oxygen consumption indicative of anaerobic glycolysis. On later CT, this area is infarcted. In the infarct, CBV is increased in relation to CBF leading to an increased transit time (TT). Due to the occlusion of the right internal carotid artery, CBF in the ipsilateral hemisphere outside the infarct is reduced without effect on CMRO2 and CMRGlc since OEF and GEF are increased

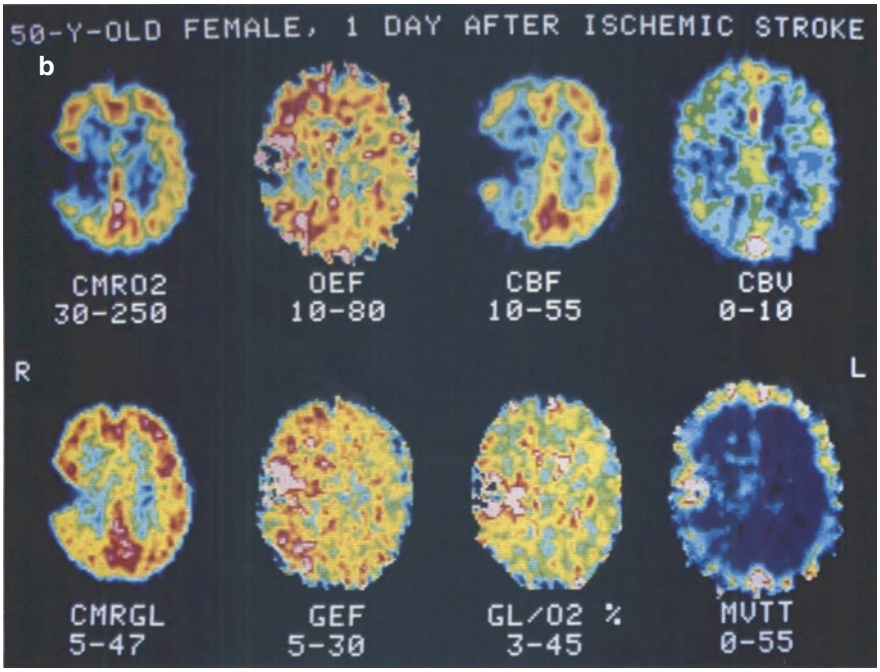

Fig. 4.11 (continued)

The impact of PET has further increased by the advent of integrated MRI-PET facilities (Broski et al. 2018; Catana et al. 2012; Portnow et al. 2013; Tondo et al. 2019; Shepherd and Nayak 2019; Shiyam Sundar et al. 2020).

Disclosures Wolf-Dieter Heiss and Olivier Zaro-Weber were funded by the WDH Foundation and the Marga and Walter Boll Foundation.

References

Attwell D, Laughlin SB (2001) An energy budget for signaling in the grey matter of the brain. J Cereb Blood Flow Metab 21(10):1133–1145

Berti V, Mosconi L, Pupi A (2014) Brain: normal variations and benign findings in fluorodeoxyglucose-PET/computed tomography imaging. PET Clin 9(2):129–140

Blomqvist G, Seitz RJ, Sjogren I, Halldin C, Stone-Elander S, Widen L et al (1994) Regional cerebral oxidative and total glucose consumption during rest and activation studied with positron emission tomography. Acta Physiol Scand 151(1):29–43

Blomqvist G, Stone-Elander S, Halldin C, Roland PE, Widen L, Lindqvist M et al (1990) Positron emission tomographic measurements of cerebral glucose utilization using [1-11C]D-glucose. J Cereb Blood Flow Metab 10(4):467–483

Bohnen NI, Djang DS, Herholz K, Anzai Y, Minoshima S (2012) Effectiveness and safety of ^{18}F-FDG PET in the evaluation of dementia: a review of the recent literature. J Nucl Med 53(1):59–71

Bonte S, Vandemaele P, Verleden S, Audenaert K, Deblaere K, Goethals I et al (2017) Healthy brain ageing assessed with ^{18}F-FDG PET and age-dependent recovery factors after partial volume effect correction. Eur J Nucl Med Mol Imaging 44(5):838–849

Broski SM, Goenka AH, Kemp BJ, Johnson GB (2018) Clinical PET/MRI: 2018 update. Am J Roentgenol 211(2):295–313

Bunevicius A, Yuan H, Lin W (2013) The potential roles of ^{18}F-FDG-PET in management of acute stroke patients. Biomed Res Int 2013:634598

Catana C, Drzezga A, Heiss WD, Rosen BR (2012) PET/MRI for neurologic applications. J Nucl Med 53(12):1916–1925

Cavaliere C, Longarzo M, Fogel S, Engstrom M, Soddu A (2020) Neuroimaging of narcolepsy and primary hypersomnias. Neuroscientist:1073858420905829

Chetelat G, Landeau B, Salmon E, Yakushev I, Bahri MA, Mezenge F et al (2013) Relationships between brain metabolism decrease in normal aging and changes in structural and functional connectivity. NeuroImage 76:167–177

Chiaravalloti A, Micarelli A, Ricci M, Pagani M, Ciccariello G, Bruno E et al (2019) Evaluation of task-related brain activity: is there a role for (18)F FDG-PET imaging? Biomed Res Int 2019:4762404

Chierichetti F, Pizzolato G (2012) ^{18}F-FDG-PET/CT. Q J Nucl Med Mol Imaging 56(2):138–150

Choo IH, Ni R, Scholl M, Wall A, Almkvist O, Nordberg A (2013) Combination of ^{18}F-FDG PET and cerebrospinal fluid biomarkers as a better predictor of the progression to Alzheimer's disease in mild cognitive impairment patients. J Alzheimers Dis 33(4):929–939

Chugani HT, Phelps ME, Mazziotta JC (1987) Positron emission tomography study of human brain functional development. Ann Neurol 22(4):487–497

Clarke D, Sokoloff L (1999) Circulation and energy metabolism of the brain. In: Siegel GJ (ed) Basic neurochemistry: molecular, cellular, and medical aspects, 6th edn. Lippincott Williams & Wilkins, Philadelphia, p xxi, 1183 p

Drzezga A (2009) Diagnosis of Alzheimer's disease with [^{18}F]PET in mild and asymptomatic stages. Behav Neurol 21(1):101–115

Drzezga A, Altomare D, Festari C, Arbizu J, Orini S, Herholz K et al (2018) Diagnostic utility of ^{18}F-Fluorodeoxyglucose positron emission tomography (FDG-PET) in asymptomatic subjects at increased risk for Alzheimer's disease. Eur J Nucl Med Mol Imaging 45(9):1487–1496

Duara R, Grady C, Haxby J, Ingvar D, Sokoloff L, Margolin RA et al (1984) Human brain glucose utilization and cognitive function in relation to age. Ann Neurol 16(6):703–713

Fox PT, Raichle ME, Mintun MA, Dence C (1988) Nonoxidative glucose consumption during focal physiologic neural activity. Science 241(4864):462–464

Garibotto V, Herholz K, Boccardi M, Picco A, Varrone A, Nordberg A et al (2017) Clinical validity of brain fluorodeoxyglucose positron emission tomography as a biomarker for Alzheimer's disease in the context of a structured 5-phase development framework. Neurobiol Aging 52:183–195

Hahn A, Gryglewski G, Nics L, Hienert M, Rischka L, Vraka C et al (2016) Quantification of task-specific glucose metabolism with constant infusion of ^{18}F-FDG. J Nucl Med 57(12):1933–1940

Hawkins RA, Phelps ME, Huang SC, Kuhl DE (1981) Effect of ischemia on quantification of local cerebral glucose metabolic rate in man. J Cereb Blood Flow Metab 1(1):37–51

Heiss WD (2009a) WSO Leadership in Stroke Medicine Award Lecture Vienna, September 26, 2008: functional imaging correlates to disturbance and recovery of language function. Int J Stroke 4(2):129–136

Heiss WD (2009b) The potential of PET/MR for brain imaging. Eur J Nucl Med Mol Imaging 36(Suppl 1):S105–S112

Heiss WD (2018) The additional value of PET in the assessment of cerebral small vessel disease. J Nucl Med 59(11):1660–1664

Heiss WD, Habedank B, Klein JC, Herholz K, Wienhard K, Lenox M et al (2004) Metabolic rates in small brain nuclei determined by high-resolution PET. J Nucl Med 45(11):1811–1815

Heiss WD, Huber M, Fink GR, Herholz K, Pietrzyk U, Wagner R et al (1992) Progressive derangement of periinfarct viable tissue in ischemic stroke. J Cereb Blood Flow Metab 12(2):193–203

Heiss WD, Pawlik G, Herholz K, Wagner R, Goldner H, Wienhard K (1984) Regional kinetic constants and cerebral metabolic rate for glucose in normal human volunteers determined by dynamic positron emission tomography of [^{18}F]-2-fluoro-2-deoxy-D-glucose. J Cereb Blood Flow Metab 4(2):212–223

Heiss WD, Pawlik G, Herholz K, Wagner R, Wienhard K (1985) Regional cerebral glucose metabolism in man during wakefulness, sleep, and dreaming. Brain Res 327(1–2):362–366

Heiss WD, Raab P, Lanfermann H (2011) Multimodality assessment of brain tumors and tumor recurrence. J Nucl Med 52(10):1585–1600

Heiss WD, Zimmermann-Meinzingen S (2012) PET imaging in the differential diagnosis of vascular dementia. J Neurol Sci 322(1–2):268–273

Herholz K (2017) Brain tumors: an update on clinical PET research in gliomas. Semin Nucl Med 47(1):5–17

Herholz K, Herscovitch P, Heiss WD (2013) NeuroPET positron emission tomography in neuroscience and clinical neurology. Springer, Berlin

Herholz K, Langen KJ, Schiepers C, Mountz JM (2012) Brain tumors. Semin Nucl Med 42(6):356–370

Hsieh TC, Lin WY, Ding HJ, Sun SS, Wu YC, Yen KY et al (2012) Sex- and age-related differences in brain FDG metabolism of healthy adults: an SPM analysis. J Neuroimaging 22(1):21–27

Jiang J, Sun Y, Zhou H, Li S, Huang Z, Wu P et al (2018) Study of the influence of age in (18) F-FDG PET images using a data-driven approach and its evaluation in Alzheimer's disease. Contrast Media Mol Imaging 2018:3786083

Jones T, Rabiner EA, Company PETRA (2012) The development, past achievements, and future directions of brain PET. J Cereb Blood Flow Metab 32(7):1426–1454

Juaristi I, Contreras L, Gonzalez-Sanchez P, Perez-Liebana I, Gonzalez-Moreno L, Pardo B et al (2019) The response to stimulation in neurons and astrocytes. Neurochem Res 44(10):2385–2391

Kalpouzos G, Chetelat G, Baron JC, Landeau B, Mevel K, Godeau C et al (2009) Voxel-based mapping of brain gray matter volume and glucose metabolism profiles in normal aging. Neurobiol Aging 30(1):112–124

Kelly PJ, Camps-Renom P, Giannotti N, Marti-Fabregas J, Murphy S, McNulty J et al (2019) Carotid plaque inflammation imaged by (18)F-Fluorodeoxyglucose positron emission tomography and risk of early recurrent stroke. Stroke 50(7):1766–1773

Kety SS, Schmidt CF (1948) The nitrous oxide method for the quantitative determination of cerebral blood flow in man: theory, procedure and normal values. J Clin Invest 27(4):476–483

Kuhl DE, Metter EJ, Riege WH, Phelps ME (1982) Effects of human aging on patterns of local cerebral glucose utilization determined by the [^{18}F]fluorodeoxyglucose method. J Cereb Blood Flow Metab 2(2):163–171

Kuwabara H, Evans AC, Gjedde A (1990) Michaelis-Menten constraints improved cerebral glucose metabolism and regional lumped constant measurements with [^{18}F]fluorodeoxyglucose. J Cereb Blood Flow Metab 10(2):180–189

Lotan E, Friedman KP, Davidson T, Shepherd TM (2020) Brain ^{18}F-FDG-PET: utility in the diagnosis of dementia and epilepsy. Isr Med Assoc J 22(3):178–184

Madsen PL, Hasselbalch SG, Hagemann LP, Olsen KS, Bulow J, Holm S et al (1995) Persistent resetting of the cerebral oxygen/glucose uptake ratio by brain activation: evidence obtained with the Kety-Schmidt technique. J Cereb Blood Flow Metab 15(3):485–491

Magistretti PJ, Allaman I (2015) A cellular perspective on brain energy metabolism and functional imaging. Neuron 86(4):883–901

Mangold R, Sokoloff L, Conner E, Kleinerman J, Therman PO, Kety SS (1955) The effects of sleep and lack of sleep on the cerebral circulation and metabolism of normal young men. J Clin Invest 34(7, Part 1):1092–1100

Marnane M, Merwick A, Sheehan OC, Hannon N, Foran P, Grant T et al (2012) Carotid plaque inflammation on ^{18}F-fluorodeoxyglucose positron emission tomography predicts early stroke recurrence. Ann Neurol 71(5):709–718

Meles SK, Renken RJ, Pagani M, Teune LK, Arnaldi D, Morbelli S et al (2020) Abnormal pattern of brain glucose metabolism in Parkinson's disease: replication in three European cohorts. Eur J Nucl Med Mol Imaging 47(2):437–450

Meyer PT, Frings L, Rucker G, Hellwig S (2017) (18)F-FDG PET in Parkinsonism: differential diagnosis and evaluation of cognitive impairment. J Nucl Med 58(12):1888–1898

Mintun MA, Lundstrom BN, Snyder AZ, Vlassenko AG, Shulman GL, Raichle ME (2001) Blood flow and oxygen delivery to human brain during functional activity: theoretical modeling and experimental data. Proc Natl Acad Sci U S A 98(12):6859–6864

Nasu S, Hata T, Nakajima T, Suzuki Y (2002) Evaluation of ^{18}F-FDG PET in acute ischemic stroke: assessment of hyper accumulation around the lesion. Kaku Igaku 39(2):103–110

Nofzinger EA, Mintun MA, Wiseman M, Kupfer DJ, Moore RY (1997) Forebrain activation in REM sleep: an FDG PET study. Brain Res 770(1-2):192–201

Pakkenberg B, Gundersen HJ (1997) Neocortical neuron number in humans: effect of sex and age. J Comp Neurol 384(2):312–320

Pardridge WM, Oldendorf WH (1977) Transport of metabolic substrates through the blood-brain barrier. J Neurochem 28(1):5–12

Patlak CS, Blasberg RG, Fenstermacher JD (1983) Graphical evaluation of blood-to-brain transfer constants from multiple-time uptake data. J Cereb Blood Flow Metab 3(1):1–7

Pawlik G, Heiss WD (1989) Positron emission tomography and neuropsychological function. In: Bigler ED, Yeo RA, Turkheimer E (eds) Neuropsychological function and brain imaging. Springer, New York, NY, pp 65–138

Phelps ME, Huang SC, Hoffman EJ, Selin C, Sokoloff L, Kuhl DE (1979) Tomographic measurement of local cerebral glucose metabolic rate in humans with (F-18)2-fluoro-2-deoxy-D-glucose: validation of method. Ann Neurol 6(5):371–388

Phelps ME, Mazziotta JC, Kuhl DE, Nuwer M, Packwood J, Metter J et al (1981) Tomographic mapping of human cerebral metabolism visual stimulation and deprivation. Neurology 31(5):517–529

Portnow LH, Vaillancourt DE, Okun MS (2013) The history of cerebral PET scanning: from physiology to cutting-edge technology. Neurology 80(10):952–956

Raichle ME, Larson KB, Phelps ME, Grubb RL Jr, Welch MJ, Ter-Pogossian MM (1975) In vivo measurement of brain glucose transport and metabolism employing glucose--^{11}C. Am J Phys 228(6):1936–1948

Raichle ME, Mintun MA (2006) Brain work and brain imaging. Annu Rev Neurosci 29:449–476

Reivich M, Alavi A, Wolf A, Fowler J, Russell J, Arnett C et al (1985) Glucose metabolic rate kinetic model parameter determination in humans: the lumped constants and rate constants for [^{18}F]fluorodeoxyglucose and [^{11}C]deoxyglucose. J Cereb Blood Flow Metab 5(2):179–192

Reivich M, Kuhl D, Wolf A, Greenberg J, Phelps M, Ido T et al (1979) The [^{18}F]fluorodeoxyglucose method for the measurement of local cerebral glucose utilization in man. Circ Res 44(1):127–137

Shen X, Liu H, Hu Z, Hu H, Shi P (2012) The relationship between cerebral glucose metabolism and age: report of a large brain PET data set. PLoS One 7(12):e51517

Shepherd TM, Nayak GK (2019) Clinical use of integrated positron emission tomography-magnetic resonance imaging for dementia patients. Top Magn Reson Imaging 28(6):299–310

Shiyam Sundar LK, Muzik O, Rischka L, Hahn A, Lanzenberger R, Hienert M et al (2020) Promise of fully integrated PET/MRI: noninvasive clinical quantification of cerebral glucose metabolism. J Nucl Med 61(2):276–284

Siesjo BK (1978) Brain energy metabolism and catecholaminergic activity in hypoxia, hypercapnia and ischemia. J Neural Transm Suppl 14:17–22

Silverman DHS, Melega WP (2004) Molecular imaging of biologic processes with PET: evaluation biologic bases of cerebral function. In: MEPD P (ed) Pet: molecular imaging and its biological applications. Springer, pp 509–583

Sokoloff L (1989) Circulation and energy metabolism of the brain. In: Siegel GJ (ed) Basic neurochemistry: molecular, cellular, and medical aspects, 4th edn. Raven Press, New York, p xviii. 984 p

Sokoloff L (1999) Energetics of functional activation in neural tissues. Neurochem Res 24(2):321–329

Sokoloff L, Reivich M, Kennedy C, Des Rosiers MH, Patlak CS, Pettigrew KD et al (1977) The [^{14}C]deoxyglucose method for the measurement of local cerebral glucose utilization: theory, procedure, and normal values in the conscious and anesthetized albino rat. J Neurochem 28(5):897–916

Tondo G, Esposito M, Dervenoulas G, Wilson H, Politis M, Pagano G (2019) Hybrid PET-MRI applications in movement disorders. Int Rev Neurobiol 144:211–257

Vaishnavi SN, Vlassenko AG, Rundle MM, Snyder AZ, Mintun MA, Raichle ME (2010) Regional aerobic glycolysis in the human brain. Proc Natl Acad Sci U S A 107(41):17757–17762

Villien M, Wey HY, Mandeville JB, Catana C, Polimeni JR, Sander CY et al (2014) Dynamic functional imaging of brain glucose utilization using fPET-FDG. NeuroImage 100:192–199

von Oertzen TJ (2018) PET and ictal SPECT can be helpful for localizing epileptic foci. Curr Opin Neurol 31(2):184–191

Wienhard K, Pawlik G, Herholz K, Wagner R, Heiss WD (1985) Estimation of local cerebral glucose utilization by positron emission tomography of [^{18}F]2-fluoro-2-deoxy-D-glucose: a critical appraisal of optimization procedures. J Cereb Blood Flow Metab 5(1):115–125

Wu HM, Bergsneider M, Glenn TC, Yeh E, Hovda DA, Phelps ME et al (2003) Measurement of the global lumped constant for 2-deoxy-2-[^{18}F]fluoro-D-glucose in normal human brain using [15O]water and 2-deoxy-2-[^{18}F]fluoro-D-glucose positron emission tomography imaging. A method with validation based on multiple methodologies. Mol Imaging Biol 5(1):32–41

Wyss MT, Jolivet R, Buck A, Magistretti PJ, Weber B (2011) In vivo evidence for lactate as a neuronal energy source. J Neurosci 31(20):7477–7485